VNU Journal of Science: Mathematics - Physics

Journal homepage: https://js.vnu.edu.vn/MaP

Original Article

Application of Anharmonic Correlated Debye Model in Investigating Anharmonic XAFS Thermodynamic Properties of Crystalline Silicon

Tong Sy Tien*

University of Fire Prevention and Fighting, 243 Khuat Duy Tien, Thanh Xuan, Hanoi, Vietnam

Received 02 April 2022
Revised 30 May 2022; Accepted 14 June 2022

Abstract: In this work, the temperature dependence of the anharmonic X-ray absorption fine structure (XAFS) and thermodynamic properties of the crystalline silicon (c-Si) have been investigated. The thermodynamic parameters are derived from the influence of the absorbing and backscattering atoms of all their nearest neighbors in the crystalline lattice with thermal vibrations. The Debye-Waller factor and thermal expansion coefficient in the anharmonic XAFS of c-Si were calculated in explicit forms using the anharmonic correlated Debye (ACD) model. This calculation model is developed from the many-body perturbation approach and correlated Debye model using the anharmonic effective potential. The numerical results of c-Si in temperature ranging from 0 to 1500 K are in good agreement with those obtained by the other theoretical procedures and experiments at several temperatures. The analytical results showed that the ACD model is useful in analyzing the experimental XAFS data on c-Si.

Keywords: XAFS Debye-Waller factor; thermal expansion coefficient; crystalline silicon; anharmonic correlated Debye model.

1. Introduction

In recent years, X-ray absorption fine structure (XAFS) has been developed into a powerful technique, and it is widely used to determine many structural parameters and dynamic properties of materials [1-4]. However, the position of atoms is not stationary, and the interatomic distance always changes due to thermal vibrations [5, 6]. These thermal vibrations are sensitive to XAFS oscillation, so

* Corresponding author.
E-mail address: tongsytien@yahoo.com

https//doi.org/10.25073/2588-1124/vnumap.4723

they cause thermal disorder and anharmonic effects on crystal vibrations and will smear out the XAFS oscillations [6, 7]. The K-edge XAFS oscillation includes a non-Gaussian disorder for a given scattering path is expressed in terms of a canonical average of all distance-dependent factors by [8-10]:

$$\chi(k)=\frac{NS_0^2(k)}{k}F(k)Im\left\{\left\langle\frac{e^{-2r/\lambda}}{r^2}\mathrm{e}^{2ikr}\right\rangle e^{i\delta(k)}\right\}, \tag{1}$$

where k is the photoelectron wavenumber, $F(k)$ is the atomic backscattering amplitude, $S_0^2(k)$ is an amplitude reduction factor, N is the coordination number, $\delta(k)$ is the net phase shift, the angular bracket $\langle\ \rangle$ is the thermal average, λ is the electron mean free path, and r depends on the temperature T and is the instantaneous distance between the backscattering and absorbing atoms.

In order to analyze the anharmonic XAFS signals caused by these thermal disorders, Bunker proposed a cumulant expansion approach to represent the anharmonic XAFS oscillation via the moments of the radial distribution (RD) function [11, 12]. In this approach, the anharmonic XAFS cumulants can be obtained by expanding a canonical average of $\left\langle\mathrm{e}^{2ikr}\right\rangle$ over many paths in the powers of k in a Taylor series [11, 13]:

$$\left\langle\mathrm{e}^{2ikr}\right\rangle=\int_0^\infty\rho(T,r)e^{2ikr}dr=\exp\left[2ikr_0+\sum_{n=1}^{\infty}\frac{(2ik)^n}{n!}\sigma^{(n)}(T)\right], \tag{2}$$

where $\sigma^{(n)}$ are nth-order cumulants, r_0 is the equilibrium distance between the backscattering and absorbing atoms, and $\rho(T,r)$ is RD function.

In investigations of the anharmonic XAFS signals, the thermal expansion (TE) coefficient $\alpha(T)$ [14, 15] and XAFS Debye-Waller (DW) factor $\mathrm{W}(T,k)$ [16, 17] are two important parameters. It is because they can characterize the anharmonic XAFS thermodynamic properties and are determined as follows [18, 19]:

$$\alpha(T)=dr/rdT\simeq d\sigma^{(1)}(T)/rdT, \tag{3}$$

$$\mathrm{W}(T,k)=\exp\left\{-2k^2\sigma^{(2)}(T)\right\}, \tag{4}$$

where the first XAFS cumulant $\sigma^{(1)}(T)$ can describe thermal lattice vibrations in the crystal lattice and significantly influences the anharmonic XAFS phase shift, and the second XAFS cumulant $\sigma^{(2)}(T)$ is the parallel mean-square relative displacement (MSRD) and can describe the anharmonic XAFS amplitude reduction.

Nowadays, crystalline silicon (c-Si) has been the most important semiconductor in the electronics and technology sectors, such as solar cells, transistors, high-power lasers**,** semiconductors, rectifiers, portland cement, fire bricks, waterproofing systems, molding compounds, ferrosilicons, and other solid-state devices, etc. [20-23]. The anharmonic XAFS cumulants of c-Si have also been investigated using the general anharmonic correlated Einstein (GACE) model [24], classical anharmonic correlated Einstein (CACE) model [25], and experiments [26]. Still, the TE coefficient and XAFS DF factor have not been fully calculated and analyzed yet in these works.

Recently, an anharmonic correlated Debye (ACD) model was efficiently used to investigate the anharmonic XAFS oscillation of many materials [27-30]. The advantage of this model is that using it one can calculate all first four cumulants, even in low-temperatures (LT) region of crystals that have low symmetry and isotropy with multiple acoustic phonons [29, 30]. Still, it has not yet been used to analyze the anharmonic XAFS oscillation of c-Si. Therefore, the calculation and analysis of the anharmonic XAFS thermodynamic properties of c-Si based on extending the ACD model will be a necessary addition to experimental data analysis in the advanced XAFS technique.

2. Formalism

Normally, Morse potential can validly affect the pair interaction (PI) potential of the crystals [31, 32]. If this potential is expanded up to the third order around its minimum position, it can be written as

$$\varphi(x) = D\left(\mathrm{e}^{-2\alpha x} - 2e^{-\alpha x}\right) \cong -D + D\alpha^2 x^2 - D\alpha^3 x^3 \tag{5}$$

where D and α are the dissociation energy and width of the potential, respectively.

To determine the thermodynamic parameters of a system, it is necessary to specify its anharmonic effective (AE) potential and force constants [33, 34]. One considers a monatomic system with an AE potential (ignoring the constant contribution) that is extended up to the third-order [13, 29]:

$$V_{eff}(x) = \frac{1}{2}k_0 x^2 - k_3 x^3, \tag{6}$$

where k_0 is the effective force constant, k_3 is the local force constant giving asymmetry of potential due to the inclusion of anharmonicity, and these local force constants are considered in the temperature-independent.

In the relative vibrations of absorbing (A) and backscattering (B) atoms, including the effect of correlation and taking into account only the nearest-neighbor interactions, the AE potential in the GACE model [35, 36] is given by:

$$V_{eff} = V(x) + \sum_{i=A,B}\sum_{j\neq A,B} V\left(\varepsilon_i x \hat{R}_{AB}\hat{R}_{ij}\right),\ \varepsilon_i = \frac{\mu}{M_i}, \tag{7}$$

where $\mu = M_A M_B / \left(M_A + M_B\right)$ is the reduced mass of the absorber and backscatter with masses M_A and M_B, respectively, $\hat{R}$ is a unit vector, $V(x)$ is a pair interaction potential of absorbing and backscattering atoms, $V\left(\varepsilon_i x \hat{R}_{AB}\hat{R}_{ij}\right)$ express the contribution of nearest-neighbor atoms to $V(x)$, the sum i is the over absorbers ($i = A$) and backscatters ($i = B$), the sum j is over the nearest neighbors.

The structural model of c-Si is illustrated in Figure 1. It can be seen that atoms are arranged with eight atoms in a diamond cubic unit cell. In this structure, all atoms are similar each to other, and each atom is bonded covalently with four other surrounding atoms in the first shell [15, 37].

Using the Morse potential in Eq. (5) to calculate the AE potential according to Eq. (7) and ignoring the overall constant, one can obtain:

$$V_{eff}(x) = V(x) + 3V\left(-\frac{1}{6}x\right) + 3V\left(\frac{1}{6}x\right) \simeq V_{eff}(x) = \frac{7}{6}D\alpha^2 x^2 - \frac{35}{36}D\alpha^3 x^3. \tag{8}$$

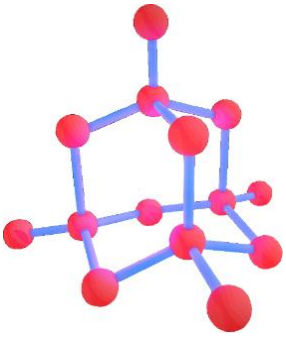

Figure 1. The structural model of c-Si.

Comparing Eq. (6) with Eq. (8), we deduce the local force constants k_0, k_3, and k_4 as follows:

$$k_0 = \frac{7}{3}D\alpha^2, \quad k_3 = \frac{35}{36}D\alpha^3. \tag{9}$$

The ACD model [27-30] is derived from the dualism of an elementary particle in quantum theory and is perfected based on the correlated Debye model [38] using the AE potential [35] and the many-body perturbation approach [39]. In this model, the atomic vibrations can be quantized and treated as a system consisting of many phonons, in which each atomic vibration corresponds to a wave that has a frequency $\omega(q)$ and is described via the dispersion relation [27, 28]:

$$\omega(q) = \omega_D \left|\sin\left(\frac{qa}{2}\right)\right|, \quad |q| \le \frac{\pi}{a}, \tag{10}$$

where q is the phonon wavenumber in the first Brillouin (FB) zone, a is the lattice constant.

In this model, the correlated Debye frequency ω_D and temperature θ_D of c-Si characterize the atomic thermal vibrations in the crystal lattice [29-30]. They can be obtained using the effective force constant k_0 from Eq. (9) as follows:

$$\omega_D = 2\sqrt{\frac{k_0}{m}} = 2\alpha\sqrt{\frac{7D}{3m}}, \tag{11}$$

$$\theta_D = \frac{\hbar\omega_D}{k_B} = \frac{2\hbar\alpha}{k_B}\sqrt{\frac{7D}{3m}}, \tag{12}$$

where ω_D can be treated using the formula $\omega_D = cq_D$, k_B is the Boltzmann constant and $\hbar$ is the reduced Planck constant.

Usually, the analysis of the temperature-dependent XAFS spectra using the cumulants is expressed in terms of the power moments of the RD function. The first and second XAFS cumulants are given by [8, 10, 40, 41]

$$\sigma^{(1)} = \langle r \rangle - r_0 = \langle x \rangle, \tag{13}$$

$$\sigma^{(2)} \equiv \sigma^2 = \left\langle \left(r - \langle r \rangle\right)^2 \right\rangle = \langle x^2 \rangle - \langle x \rangle^2, \tag{14}$$

where, $x = r - r_0$ is the deviation distance between the backscattering and absorbing atoms, the first XAFS cumulant relates to the centroid of real RD function, and the second XAFS cumulant characterizes the variance of real RD function.

The general expressions of the anharmonic XAFS cumulants in the ACD model were calculated in the temperature dependence by Hung et al., [27]. Still, these obtained expressions are not optimized yet because they depend on the lattice constant *a* [30]. Therefore, we have extended the previous ACD model to calculate the temperature-dependent TE coefficient and XAFS DW factor of c-Si. After substituting the expressions of local force constants k_0 and k_3 of c-Si in Eq. (9) into these general expressions [27] and converting from variable q to variable p in the formula $p = qa/2$, we obtain the temperature-dependent first and second XAFS cumulants in the form as:

$$\sigma^{(1)}(T) = \frac{15\hbar}{28\pi D\alpha}\int_0^{\pi/2}\omega(p)\frac{1+\exp\{-\hbar\omega(p)/k_BT\}}{1-\exp\{-\hbar\omega(p)/k_BT\}}dp$$

$$= \frac{15\hbar}{28\pi D\alpha}\int_0^{\pi/2}\omega(p)\coth\{\hbar\omega(p)/2k_BT\}dp, \quad (15)$$

$$\sigma^{2}(T) = \frac{3\hbar}{7\pi D\alpha^2}\int_0^{\pi/2}\omega(p)\frac{1+\exp\{-\hbar\omega(p)/k_BT\}}{1-\exp\{-\hbar\omega(p)/k_BT\}}dp$$

$$= \frac{3\hbar}{7\pi D\alpha^2}\int_0^{\pi/2}\omega(p)\coth\{\hbar\omega(p)/2k_BT\}dp, \quad (16)$$

Substituting these cumulants into the Eqs. (3) and (4) to calculate the temperature-dependent TE coefficient and XAFS DW factor of c-Si, we obtain the following results:

$$\alpha(T) = \frac{15\hbar}{28\pi D\alpha r}d\left\{\int_0^{\pi/2}\omega(p)\coth\{\hbar\omega(p)/2k_BT\}dp\right\}\Big/dT, \quad (17)$$

$$\mathrm{W}(T,k) = \exp\left\{-\frac{6\hbar k^2}{7\pi D\alpha^2}\int_0^{\pi/2}\omega(p)\coth\{\hbar\omega(p)/2k_BT\}dp\right\}. \quad (18)$$

Using the approximations $\exp\{-\hbar\omega(p)/k_BT\} \approx 0$, we calculate the TE coefficient and XAFS DW factor of c-Si in the LT limit ($T \to 0$) from Eqs. (17) and (18). The obtained results are

$$\alpha(T) \simeq \frac{5\pi k_B^2 T}{14\hbar r\omega_D D\alpha}, \quad (19)$$

$$\mathrm{W}(T,k) \simeq \exp\left\{-\frac{4\sqrt{21}\hbar k^2}{7\pi\alpha\sqrt{Dm}}\right\}. \quad (20)$$

Using the approximation $\exp\{-\hbar\omega(p)/k_BT\} \approx 1-\hbar\omega(p)/k_BT$, we calculate the TE coefficient and XAFS DW factor of c-Si in the high-temperature (HT) limit ($T \to \infty$) from Eqs. (17) and (18). The obtained results are

$$\alpha(T) = \frac{15k_B}{28D\alpha r}, \quad (21)$$

$$\mathrm{W}(T,k)=\exp\left\{-\frac{6k_BTk^2}{7D\alpha^2}\right\}. \quad (22)$$

Thus, an extended ACD model has been perfected to efficiently calculate the temperature dependence of TE coefficient and XAFS DF factor of c-Si. The obtained expressions using this model can satisfy all their fundamental properties in the temperature dependence. These expressions have also been optimized to not depend on the lattice constant as in the previous ACD model.

3. Result and Discussion

In this section, the obtained expressions using the ACD model in Sec. 2 are applied to the numerical calculations of c-Si. In these calculations, we use the atomic mass $m=28.09$ u [42] and Morse potential parameters $D=1.83$ eV, $\alpha=1.56$ Å^{-1}, and $r_0=2.34$ Å [43] to calculate the local force constants, the correlated Debye frequency and temperature, the wavenumber-dependent frequency, the position-dependent AE potential, the temperature-dependent first and second XAFS cumulants and TE coefficient, and the wavenumber-dependent XAFS DF factor. Our obtained numerical results are compared with those obtained using the GACE [24], CACE [25] models, a fitting method [44], and experiments [26, 45]. From these obtained comparisons, we analyze and discuss the development and effectiveness of the ACD model in investigating anharmonic XAFS thermodynamic properties of c-Si. The following is the presentation of our numerical results:

Using Eq. (9), (11), and (12) in the ACD model, we calculate the local force constants $k_0\simeq10.39$ eVÅ^{-2}, $k_3\simeq6.75$ eVÅ^{-3}, and $k_4\simeq6.35$ eVÅ^{-4}, the correlated Debye frequency $\omega_D\simeq1.19\times10^{14}$ Hz, and the correlated Debye temperature $\theta_D\simeq910.05$ K.

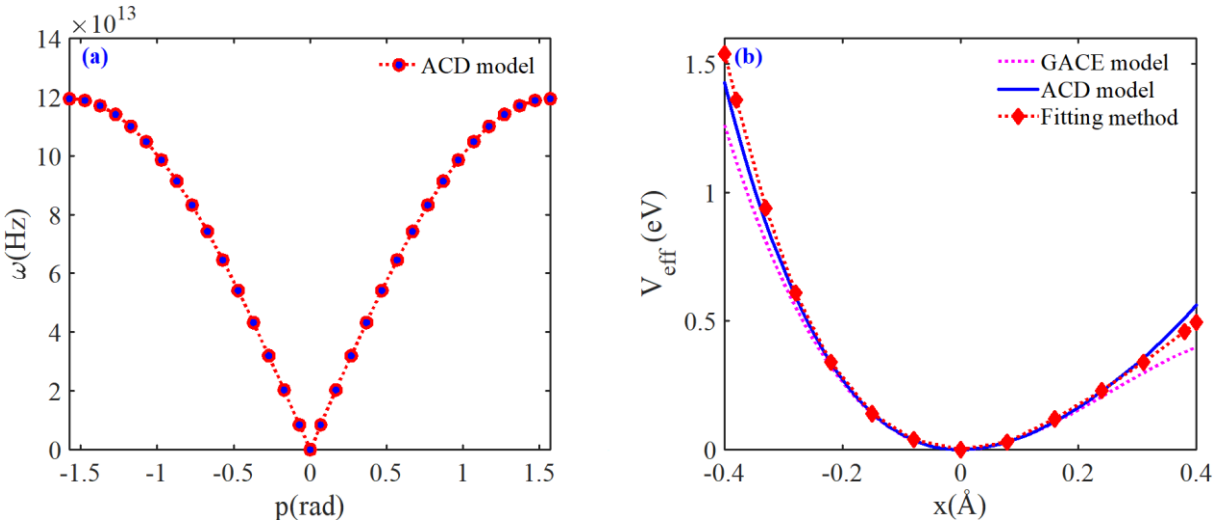

Figure 2. The wavenumber-dependent frequency (a) and The position-dependent AE potential of c-Si obtained from the ACD and GACE [24] models and a fitting method [44] (b).

The wavenumber dependence of the frequency of c-Si in the FB zone is calculated by Eq. (10) and is represented in Figure 2a. It can be shown that our obtained frequency using the ACD is a

symmetric function of a linear chain of q, and its maximum value is ω_D at the bounds of the FB zone with $q = \pm\pi / a$. Also, the position dependence of the AE potential of c-Si in the position range from -0.4 to 0.4 Å is represented in Figure 2b. Herein, our obtained result using the ACD model is calculated by Eq. (8), while those obtained using the GACE model [24] do not take into account the fourth anharmonic term in this equation. In comparison with the obtained result from a reactive empirical bond-order potential of c-Si by fitting its bond-order terms [44], it can be seen that our result is better agreement with those obtained using the GACE model [24], especially at positions far from the minimum position. Moreover, the obtained result using the CACE model [25] is similar to our result because in this model Eq. (8) is also used for calculations.

The temperature dependence of the first XAFS cumulant $\sigma^{(1)}(T)$ and the second XAFS cumulant $\sigma^2(T)$ of c-Si in a range from 0 to 1500 K is presented in Fig. 3.

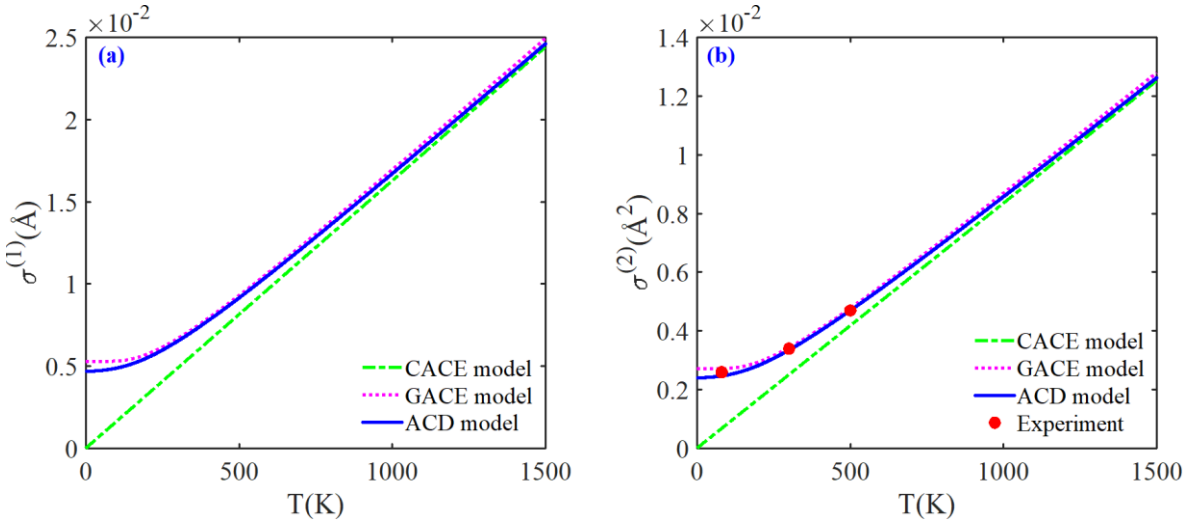

Figure 3. The temperature-dependent (a) first and (b) second XAFS cumulants of c-Si obtained using the ACD, GACE [24], and CACE [25] models and experiment [26].

Herein, our obtained results using the ACD model are calculated by Eqs. (15) and (16), and the experimental values at 80 K, 300 K, and 500 K are measured at the Synchrotron Radiation Center by Benfatto *et al*. It can be seen that our results are in good agreement with those obtained using the GACE [24] and CACE (only at the high temperatures) [25] models and experiment [26]. For example, the obtained results using the ACD model, GACE model [24], CACE model [25], and experiment [26] at $T = 300$ K are $\sigma^{(1)} \simeq 6.54\times10^{-3}$ Å and $\sigma^2 \simeq 3.36\times10^{-3}$ Å², $\sigma^{(1)} \simeq 6.67\times10^{-3}$ Å and $\sigma^2 \simeq 3.43\times10^{-3}$ Å², $\sigma^{(1)} \simeq 4.88\times10^{-3}$ Å and $\sigma^2 \simeq 2.50\times10^{-3}$ Å², and $\sigma^2 \simeq 3.40\times10^{-3}$ Å², respectively. Moreover, it can be seen that the obtained results using the CACE model [25] approach zero as the temperature approaches zero, so this model can not work well in the LT region. It is because the CACE model [25] cannot calculate quantum effects using classical statistical theory. Meanwhile, the ACD and GACE [24] models both show quantum effect contributions, but the obtained results using the GACE model [24] in the LT region are slightly greater. It can be explained because the GACE model [24] uses only one effective frequency to describe the atomic thermal vibrations, as seen in Figure 3.

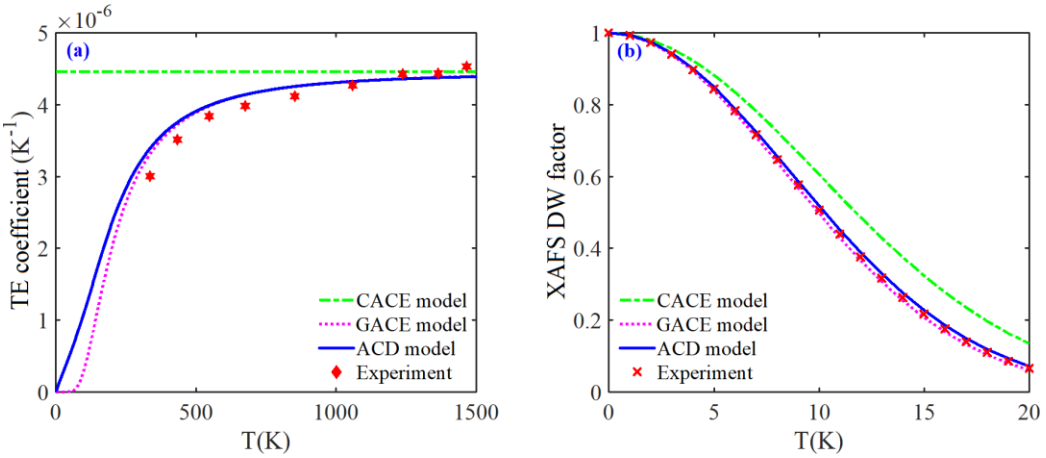

Figure 4. (a) The temperature-dependent TE coefficient and (b) the wavenumber-dependent XAFS DW factor at 500 K of c-Si obtained using the ACD, GACE [24], CACE [25] models and experiments [26, 45].

The temperature dependence of the TE coefficient of c-Si in a temperature range from 0 to 1500 K is shown in Figure 4a. Our obtained result using the ACD model is calculated by Eq. (17), while the experimental values are measured in a high-temperature furnace by Okada & Tokumaru [26]. It can be seen that our result agrees with those obtained using the GACE [24] and CACE (only in the HT region) [25] models and experiments [45]. For example, the obtained results using the ACD model, GACE model [24], CACE model [25], and experiment [45] at T = 546 K, are $\alpha = 3.98 \times 10^{-6}K^{-1}$, $\alpha = 3.96 \times 10^{-6}K^{-1}$, $\alpha = 4.46 \times 10^{-6}K^{-1}$, and $\alpha = 3.74 \times 10^{-6}K^{-1}$respectively.

Herein, the obtained results using the GACE and CACE models are calculated by Eq. (3), with the temperature-dependent first XAFS cumulant determined in [24] and [25], respectively. Moreover, our result is not destroyed as those obtained using the GACE in the LT limit and fits perfectly with Eq. (19), which indicates that the ACD model can fully describe quantum effects. Also, our results increase with increasing temperature *T* and approach those obtained using the CACE model [25] in the HT limit, which fits perfectly with Eq. (21) and shows that the ACD model can efficiently describe the anharmonic effects. Meanwhile, the obtained result using the CACE model [25] is constant because the temperature-dependent first XAFS cumulant is a linear function in this model, as seen in Eq. (21) and Figure 4a.

The wavenumber dependence of the XAFS DW factor of c-Si at 500 K and in a range from 0 to 20 Å is represented in Figure 4b. Our obtained result using the ACD model is calculated by Eq. (18), while the obtained results using the experiment are calculated by Eq. (4) with the experimental value of the second XAFS cumulant. It can be seen that our result agrees with those obtained using the GACE model [24] and experiment [26], and our result is more experimentally agree than those obtained using the CACE model [25] because this model only works well at high temperatures. For example, the obtained results using the ACD model, GACE model [24], and CACE model [25], and experiment [26] at $T = 300$ K with $k = 10$ Å^{-1} and 20 Å^{-1}, are $W \simeq 0.52$ and 0.07, $W \simeq 0.50$ and 0.06, $W \simeq 0.61$ and 0.14, and $W \simeq 0.51$ and 0.06, respectively, while the corresponding results at $T = 500$ K are $W \simeq 0.40$ and 0.03, $W \simeq 0.38$ and 0.02, $W \simeq 0.43$ and 0.04, and $W \simeq 0.39$ and 0.02, respectively. Herein, the obtained results using the GACE and CACE model are calculated by Eq. (4), with the temperature-dependent second XAFS cumulant determined in [24, 25]. Moreover, It can be seen that the values of the XAFS DW factor decrease with increasing temperature and decrease with fast-increasing wavenumber *k*. It is because the XAFS DW factor is an inverse function of the wavenumber *k*

and second XAFS cumulant $\sigma^{(2)}(T)$, in which this cumulant increases with increasing temperature, as seen in Eq. (4) and Figure 3b.

Thus, the calculated results of the anharmonic TE coefficient and XAFS DW factor using the present ACD model satisfied all of their fundamental properties. The TE coefficient increases with increasing temperature and the XAFS DW factor decreases with increasing temperature. It means that the crystalline lattice expands strongly, and the XAFS amplitude decreases more strongly at higher temperatures. These results can also describe the influence of anharmonic effects at high temperatures and the influence of quantum effects at low temperatures.

4. Conclusion

In this work, we have performed the expansion and development of an efficient model to calculate and analyze the anharmonic XAFS thermodynamic properties of c-Si. The calculated results of the anharmonic TE coefficient and XAFS DW factor using the ACD model satisfied all of their fundamental properties in the temperature dependence. The TE coefficient increases with increasing temperature, and the XAFS DW factor decreases with increasing temperature. It means that the crystalline lattice expands strongly, and the XAFS amplitude decreases more strongly at higher temperatures. These results can also describe the influence of anharmonic effects at high temperatures and the influence of quantum effects at low temperatures on the XAFS thermodynamic properties.

A good agreement of our numerical results of c-Si with those obtained using the GACE model, CACE model, and experiments at various temperatures showed the effectiveness of the present model in investigating the anharmonic XAFS thermodynamic properties. This model can be applied to calculate and analyze the anharmonic TE coefficient and XAFS DW factor of other crystals from above absolute zero temperature to just before the melting point.

Acknowledgments

The author would like to thank Prof. Nguyen Van Hung (VNU Hanoi, Vietnam) for their helpful discussions and comments on the anharmonic XAFS theory. This work was supported by the University of Fire Prevention and Fighting, 243 Khuat Duy Tien, Thanh Xuan, Hanoi, Vietnam.

References

[1] P. Fornasini, R. Grisenti, M. Dapiaggi, G. Agostini, T. Miyanaga, Nearest-neighbour Distribution of Distances in Crystals from Extended X-ray Absorption Fine Structure, Journal of Chemical Physics, Vol. 147, No. 4, 2017, pp. 044503, https://doi.org/10.1063/1.4995435.

[2] F. D. Vila, J. W. Spencer, J. J. Kas, J. J. Rehr, F. Bridges, Extended X-Ray Absorption Fine Structure of ZrW2O8: Theory vs. Experiment, Frontiers in Chemistry, Vol. 6, 2018, pp. 356, https://doi.org/10.3389/fchem.2018.00356.

[3] T. Yokoyama, S. Chaveanghong, Anharmonicity in Elastic Constants and Extended X-ray-absorption Fine Structure Cumulants, Physical Review Materials, Vol. 3, 2019, pp. 033607, https://doi.org/10.1103/PhysRevMaterials.3.033607.

[4] J. J. Rehr, F. D. Vila, J. J. Kas, N. Y. Hirshberg, K. Kowalski, B. Peng, Equation of Motion Coupled-cluster Cumulant Approach for Intrinsic Losses in X-ray Spectra, Journal of Chemical Physics, Vol. 152, 2020, pp. 174113, https://doi.org/10.1063/5.0004865.

[5] E. A. Stern, B. A. Bunker, S. M. Heald, Many-body Effects on Extended X-ray Absorption Fine Structure Amplitudes, Physical Review B, Vol. 21, No. 12, 1980, pp. 5521-5539, https://doi.org/10.1103/PhysRevB.21.5521.
[6] P. A. Lee, P. H. Citrin, P. Eisenberger, B. M. Kincaid, Extended X-ray Absorption Fine Structure Its Strengths and Limitations as A Structural Tool, Reviews of Modern Physics, Vol. 53, No. 4, 1981, pp. 769-806, https://doi.org/10.1103/RevModPhys.53.769.
[7] P. Eisenberger, G. S. Brown, The Study of Disordered Systems by EXAFS: Limitations, Solid State Communications, Vol. 29, No. 6, 1979, pp. 481-484, https://doi.org/10.1016/0038-1098(79)90790-7.
[8] J. J. Rehr, R. C. Albers, Theoretical Approaches to X-ray Absorption Fine Structure, Reviews of Modern Physics, Vol. 72, No. 3, 2000, pp. 621-654, https://doi.org/10.1103/RevModPhys.72.621.
[9] J. M. Tranquada, R. Ingalls, Extended X-ray Absorption Fine-structure Study of Anharmonicity in CuBr, Physical Review B, Vol. 28, No. 6, 1983, pp. 3520-3528, https://doi.org/10.1103/PhysRevB.28.3520.
[10] E. D. Crozier, J. J. Rehr, R. Ingalls, Amorphous and Liquid Systems, in: D. C. Koningsberger, R. Prins (Eds.), X-ray Absorption: Principles, Applications, Techniques of XAFS, SXAFS and XANES, John Wiley & Sons, New York, 1988. pp. 373-442, https://www.wiley.com/en-gb/exportProduct/pdf/9780471875475 (accessed on: May 1st, 2022).
[11] G. Bunker, Application of the Ratio Method of EXAFS Analysis to Disordered Systems, Instruments and Methods in Physics Research, Vol. 207, No. 3. 1983, pp. 437-444, https://doi.org/10.1016/0167-5087(83)90655-5.
[12] L. Tröger, T. Yokoyama, D. Arvanitis, T. Lederer, M. Tischer, K. Baberschke, Determination of Bond Lengths, Atomic Mean-square Relative Displacements, and Local Thermal Expansion By Means of Soft-x-ray Photoabsorption, Physical Review B, Vol. 49, No. 2, 1994, pp. 888-903, https://doi.org/10.1103/PhysRevB.49.888.
[13] T. Yokoyama, K. Kobayashi, T. Ohta, A. Ugawa, Anharmonic Interatomic Potentials of Diatomic and Linear Triatomic Molecules Studied by Extended X-ray Absorption Fine Structure, Physical Review B, Vol. 53, No. 10, 1996, pp. 6111-6122, https://doi.org/10.1103/PhysRevB.53.6111.
[14] P. A. Tipler, G. Mosca, Physics for Scientists and Engineers, Sixth ed., Macmillan Learning, New York, 2004, pp. 666-670, https://www.webassign.net/features/textbooks/tipler6/details.html (accessed on: May 1st, 2022).
[15] C. Kittel, Introduction to Solid State Physics, Eighth ed., John Wiley & Sons, New York, 2004, https://www.academia.edu/38635861/Introduction_to_Solid_State_Physics_Charles_Kittel (accessed on: May 1st, 2022).
[16] F. W. Lytle, D. E. Sayers, E. A. Stern, Extended X-ray-absorption Fine-structure Technique. II. Experimental practice and selected results, Physical Review B, Vol. 11, No. 12, 1975, pp. 4825-4835, https://doi.org/10.1103/PhysRevB.11.4825.
[17] R. B. Greegor, F. W. Lytle, Extended X-ray Absorption Fine Structure Determination of Thermal Disorder in Cu: Comparison of theory and experiment, Physical Review B, Vol. 20, No. 12, 1979, pp. 4902-4907, https://doi.org/10.1103/PhysRevB.20.4902.
[18] N. V. Hung, C. S. Thang, N. B. Duc, D. Q. Vuong, T. S. Tien, Temperature Dependence of Theoretical and Experimental Debye-Waller Factors, Thermal Expansion and XAFS of Metallic Zinc, Physica B: Condensed Matter, Vol. 521, 2017, pp. 198-203, http://dx.doi.org/10.1016/j.physb.2017.06.027.
[19] N. V. Hung, C. S. Thang, N. B. Duc, D. Q. Vuong, T. S. Tien, Advances in Theoretical and Experimental XAFS Studies of Thermodynamic Properties, Anharmonic Effects and Structural Determination of Fcc Crystals, European Physical Journal B, Vol. 90, 2017, pp. 256, https://doi.org/10.1140/epjb/e2017-80383-1.
[20] M. G. Voronkov, Silicon era, Russian Journal of Applied Chemistry, Vol. 80, No. 12, 2007, pp. 2190-2196, https://doi.org/10.1134/S1070427207120397.
[21] E. Epstein, Silicon, Annual Review of Plant Physiology and Plant Molecular Biology, Vol. 50, 1999, pp. 641-664, https://doi.org/10.1146/annurev.arplant.50.1.641.
[22] J. Emsley, Nature's Building Blocks: An A-Z Guide to the Elements, Second ed., Oxford University Press, New York, 2011, https://archive.org/details/naturesbuildingb0000emsl (accessed on: May 1st, 2022).
[23] W. Heywang, K. H. Zaininger, Silicon: the Semiconductor Material, in: P. Siffert, E. F. Krimmel (Eds.), Silicon: Evolution and Future of a Technology, Springer Verlag, Heidelberg, 2004, pp. 25-42, https://doi.org//10.1007/978-3-662-09897-4_2.
[24] N. V. Hung, N. B. Duc, D. Q. Vuong, N. C. Toan, T. S. Tien, Advances in EXAFS Studies of Thermodynamic Properties and Anharmonic Effects Based on Debye-waller Factors, Applications to Semiconductors, Vacuum, Vol. 169, 2019, pp. 108872, https://doi.org/10.1016/j.vacuum.2019.108872.
[25] T. S. Tien, L. V. Hoang, Temperature Dependence of Anharmonic EXAFS Oscillation of Crystalline Silicon, Journal of Tan Trao University, Vol. 6, No. 19, 2020, pp. 95-102, https://doi.org/10.51453/2354-1431/2020/435.

[26] M. Benfatto, C. R. Natoli, A. Filipponi, Thermal and Structural Damping of the Multiple-Scattering Contributions to the X-ray-absorption Coefficient, Physical Review B, Vol. 40, No. 14, 1991, pp. 9626-9635, https://doi.org/10.1103/PhysRevB.40.9626.
[27] N. V. Hung, N. B. Trung, B. Kirchner, Anharmonic Correlated Debye Model Debye-waller Factors, Physica B: Condensed Matter, Vol. 405, No. 11, 2010, pp. 2519-2525, https://doi.org/10.1016/j.physb.2010.03.013.
[28] N. V. Hung, T. T. Hue, H. D. Khoa, D. Q. Vuong, Anharmonic Correlated Debye Model High-order Expanded Interatomic Effective Potential and Debye-waller Factors of Bcc Crystals, Physica B: Condensed Matter, Vol. 503, No. 15, 2016, pp. 174-178, http://dx.doi.org/10.1016/j.physb.2016.09.019.
[29] T. S. Tien, Analysis of EXAFS Oscillation of Monocrystalline Diamond-semiconductors Using Anharmonic Correlated Debye Model, European Physical Journal Plus, Vol. 136, 2021, pp. 539, https://doi.org/10.1140/epjp/s13360-021-01378-z.
[30] T. S. Tien, Effect of The Non-Ideal Axial Ratio C/A on Anharmonic EXAFS Oscillation of H.C.P. Crystals, Journal of Synchrotron Radiation, Vol. 28, 2021, pp. 1544-1557, https://doi.org/10.1107/S1600577521007256.
[31] P. M. Morse, Diatomic Molecules According to the Wave Mechanics, II. Vibrational Levels, Physical Review, Vol. 34, 1929, pp. 57-64, https://doi.org/10.1103/PhysRev.34.57.
[32] L. A. Girifalco, V. G. Weizer, Application of the Morse Potential Function to Cubic Metals, Physical Review, Vol. 114, No. 3, 1959, pp. 687-690, https://doi.org/10.1103/PhysRev.114.687.
[33] N. V. Hung, L. H. Hung, T. S. Tien, R. R. Frahm, Anharmonic effective potential, effective local force constant and EXAFS of hcp crystals: Theory and comparison to experiment, International Journal *of* Modern Physics B, Vol. 22, No. 29, 2008, pp. 5155-5166, https://doi.org/10.1142/S0217979208049285.
[34] N. V. Hung, T. S. Tien, N. B. Duc, D. Q. Vuong, High-order Expanded XAFS Debye-Waller Factors of HCP crystals based on classical anharmonic correlated Einstein model, Modern Physics Letters B, Vol. 28, No. 21, 2014, pp. 1450174, https://doi.org/10.1142/S0217984914501747.
[35] N. V. Hung, J. J. Rehr, Anharmonic correlated Einstein-model Debye-Waller factors, Physical Review B, Vol. 56, No. 1, 1997, pp. 43-46, https://doi.org/10.1103/PhysRevB.56.43.
[36] N. V. Hung, P. Fornasini, Anharmonic Effective Potential, Correlation Effects, and EXAFS Cumulants Calculated from a Morse Interaction Potential for fcc Metals, Journal of the Physical Society of Japan, Vol. 76, No. 8, 2007, pp. 084601, https://doi.org/10.1143/JPSJ.76.084601.
[37] S. H. Simon, The Oxford Solid State Basics, First ed., Oxford University Press, Oxford, 2013, https://www-thphys.physics.ox.ac.uk/people/SteveSimon/book.html (accessed on: May 1st, 2022).
[38] G. Beni, P. M. Platzman, Temperature and Polarization Dependence of Extended X-ray Absorption Fine-structure Spectra, Physical Review B, Vol. 14, No. 4, 1976, pp. 1514-1518, https://doi.org/10.1103/PhysRevB .14.1514.
[39] G. D. Mahan, Many-Particle Physics, Second ed., Plenum, New York, 1990, https://doi.org/10.1007/978-1-4613-1469-1.
[40] T. S. Tien, Advances in studies of the temperature dependence of the EXAFS amplitude and phase of FCC crystals, Journal of Physics D Applied Physics, Vol. 53, No. 11, 2020, pp. 315303, https://doi.org/10.1088/1361-6463/ab8249.
[41] T. S. Tien, Investigation of the Anharmonic EXAFS Oscillation of Distorted HCP Crystals Based on Extending Quantum Anharmonic Correlated Einstein Model, Japanese Journal of Applied Physics, Vol. 60, 2021, pp. 112001, https://doi.org/10.35848/1347-4065/ac21b3.
[42] P. Chaloner, Organic Chemistry: A Mechanistic Approach, First ed., CRC Press, Boca Raton, 2015, https://doi.org/10.1201/b17689.
[43] R. A. Swalin, Theoretical Calculations of the Enthalpies and Entropies of Diffusion and Vacancy Formation in Semiconductors, Journal of Physics and Chemistry of Solids, Vol. 18, No. 4, 1961, pp. 290-296, https://doi.org/10.1016/0022-3697(61)90120-2.
[44] J. D. Schall, G. Gao, J. A. Harrison, Elastic Constants of Silicon Materials Calculated as A Function of Temperature Using A Parametrization of the Second-generation Reactive Empirical Bond-order Potential, Physical Review B, Vol. 77, 2008, pp. 115209, https://doi.org/10.1103/PhysRevB.77.115209.
[45] Y. Okada, Y. Tokumaru, Precise determination of Lattice Parameter and Thermal Expansion Coefficient of Silicon between 300 and 1500 K, Journal of Applied Physics, Vol. 56, No. 2, 1984, pp. 314-320, http://dx.doi.org/10.1063/1.333965.